The Dixenon(1+) Cation: Formation in the Condensed Phases and Characterization by ESR, UV–Visible, and Raman Spectroscopy†

Dean R. Brown,[1a] Martin J. Clegg,[1a] Anthony J. Downs,*[,1a] Richard C. Fowler,[1a] Alan R. Minihan,[1a] James R. Norris,[1b] and Lawrence Stein[1b]

Inorganic Chemistry Laboratory, University of Oxford, Oxford, OX1 3QR, U.K., and Chemistry Division, Argonne National Laboratory, Argonne, Illinois 60439

Received March 11, 1992

The redox chemistry of the couple formed by XeF^+ and elemental xenon gives rise to a green intermediate. This is formed, for example, from $XeF^+Sb_2F_{11}^-$ in antimony pentafluoride solution, irreversibly under the action of various reducing agents (e.g. H_2O, Pb, Hg, SO_2, PF_3, or SbF_3) or reversibly under the action of xenon gas, and while an overpressure of xenon is maintained, it is long-lived at ambient temperatures. The product has been characterized by a combination of ESR, UV–visible, and Raman spectroscopies, enrichment in ^{136}Xe or ^{129}Xe playing a crucial role in establishing that the carrier of the green coloration is the dixenon(1+) cation, Xe_2^+. Quantitative studies of the UV–visible and Raman spectra of antimony pentafluoride solutions imply that the reversible formation of Xe_2^+ takes place in accordance with the equilibrium $3Xe + XeF^+Sb_2F_{11}^- + 2SbF_5 \rightleftarrows 2Xe_2^+Sb_2F_{11}^-$, although a secondary equilibrium finds the Xe_2^+ bound in a complex with an excess of the oxidant: $Xe_2^+Sb_2F_{11}^- + XeF^+Sb_2F_{11}^- \rightleftarrows Xe_2^+Sb_2F_{11}^-\cdot XeF^+Sb_2F_{11}^-$. The spectroscopic properties of Xe_2^+ are discussed in relation to those of the isoelectronic species I_2^- and to the results of previous theoretical calculations. Of the media investigated to date antimony pentafluoride seems to be unique in its ability to support the Xe_2^+ cation in appreciable concentrations at normal temperatures.

Introduction

Compounds in which xenon assumes a formal oxidation state less than +2 are typically weakly bound and short-lived under normal conditions. Some of them, like XeF, XeCl, and Xe_2Cl, have commanded much attention through their formation as diatomic or triatomic exciplexes with the capacity, real or potential, to develop useful laser action.[2,3] Such species can be photogenerated in the solid, liquid, or gas phases and characterized, most commonly by their optical emission spectra[4-6] but sometimes also by absorption[6] and ESR[7] measurements. Certain of them—most notably XeF—have been invoked as intermediates in redox reactions of xenon and its compounds.[8]

Although the cation Xe^+ is certainly formed in the gas phase, its existence as a recognizable, long-lived component of the condensed phases has yet to be verified. This is puzzling when one recalls that solids with the compositions $XePtF_6$ and $XeRhF_6$ were among the first isolable chemical derivatives of xenon to be described, yet the natures of these solids remain to be elucidated.[9] That the dixenon(1+) cation, Xe_2^+, is also formed in the gas phase, for example by reaction 1, has been established mass

$$Xe + Xe^+ + M \rightarrow Xe_2^+ + M \quad (M = \text{third body}) \quad (1)$$

spectrometrically,[10a] by photoionization measurements,[10b] photoelectron spectroscopy,[10c] and differential elastic scattering.[10d] With other noble gas dimer ions, it has been the subject of several theoretical studies.[11] Despite the interest which it has thus evinced

† This paper is dedicated by A.J.D. out of friendship and scientific regard to Professor Dr. mult. Alois Haas of the Ruhr-Universität Bochum on the occasion of his 60th birthday.

(1) (a) University of Oxford. (b) Argonne National Laboratory.

(2) Andrews, D. L. *Lasers in Chemistry*; Springer-Verlag: Berlin, Heidelberg, 1986. Demtröder, W. *Laser Spectroscopy: Basic Concepts and Instrumentation*; Springer-Verlag: Berlin, Heidelberg, 1981. Wilson, J.; Hawkes, J. F. B. *Lasers: Principles and Applications*; Prentice Hall: Hemel Hempstead, U.K., 1987. Rhodes, Ch. K., Ed. *Excimer Lasers*; Topics in Applied Physics, Vol. 30; Springer-Verlag: Berlin, Heidelberg, 1979.

(3) Fajardo, M. E.; Withnall, R.; Feld, J.; Okada, F.; Lawrence, W.; Wiedeman, L.; Apkarian, V. A. *Laser Chem.* **1988**, *9*, 1.

(4) See, for example, the following: Fajardo, M. E.; Apkarian, V. A. *J. Chem. Phys.* **1986**, *85*, 5660. Wiedeman, L.; Fajardo, M. E.; Apkarian, V. A. *Chem. Phys. Lett.* **1987**, *134*, 55. Last, I.; George, T. F.; Fajardo, M. E.; Apkarian, V. A. *J. Chem. Phys.* **1987**, *87*, 5917. Wiedeman, L.; Fajardo, M. E.; Apkarian, V. A. *J. Phys. Chem.* **1988**, *92*, 342. Fajardo, M. E.; Apkarian, V. A. *J. Chem. Phys.* **1988**, *89*, 4102. Katz, A. I.; Apkarian, V. A. *J. Phys. Chem.* **1990**, *94*, 6671. Okada, F.; Apkarian, V. A. *J. Chem. Phys.* **1991**, *94*, 133.

(5) Goodman, J.; Brus, L. E. *J. Chem. Phys.* **1976**, *65*, 3808. Monahan, K. M.; Jones, V. O.; Rehn, V. *J. Chem. Phys.* **1979**, *71*, 2360.

(6) Ault, B. S.; Andrews, L. *J. Chem. Phys.* **1976**, *65*, 4192. Ault, B. S.; Andrews, L.; Green, D. W.; Reedy, G. T. *J. Chem. Phys.* **1977**, *66*, 2786. Goetschalckx, M. A.; Mowery, R. L.; Krausz, E. R.; Yeakel, W. C.; Schatz, P. N.; Ault, B. S.; Andrews, L. *Chem. Phys. Lett.* **1977**, *47*, 23.

(7) (a) Morton, J. R.; Falconer, W. E. *J. Chem. Phys.* **1963**, *39*, 427. Eachus, R. S.; Symons, M. C. R. *J. Chem. Soc. A* **1971**, 304. Yakimchenko, O. E.; Degtyarov, E. N.; Prusakov, V. N.; Lebedev, Ya. S. *Chem. Phys. Lett.* **1980**, *72*, 373. (b) Falconer, W. E.; Morton, J. R.; Streng, A. G. *J. Chem. Phys.* **1964**, *41*, 902. (c) Adrian, F. J.; Bowers, V. A. *J. Chem. Phys.* **1976**, *65*, 4316. (d) Boate, A. R.; Morton, J. R.; Preston, K. F. *Chem. Phys. Lett.* **1978**, *54*, 579.

(8) Legasov, V. A.; Prusakov, V. N.; Chaivanov, B. B. *Russ. J. Phys. Chem.* **1968**, *42*, 610. Johnston, H. S.; Woolfolk, R. *J. Chem. Phys.* **1964**, *41*, 269. Baker, B. G.; Fox, P. G. *Nature* **1964**, *204*, 466. Weaver, E. E.; Weinstock, B.; Knop, C. P. *J. Am. Chem. Soc.* **1963**, *85*, 111. Bartlett, N.; Wechsberg, M.; Sladky, F. O.; Bulliner, P. A.; Jones, G. R.; Burbank, R. D. *J. Chem. Soc., Chem. Commun.* **1969**, 703.

(9) Bartlett, N. *Proc. Chem. Soc.* **1962**, 218. Hyman, H. H., Ed. *Noble-Gas Compounds*; The University of Chicago Press: Chicago, 1963. Holloway, J. H. *Noble-Gas Chemistry*; Methuen: London, 1968. Bartlett, N.; Sladky, F. O. In *Comprehensive Inorganic Chemistry*; Bailar, J. C., Jr., Emeléus, H. J., Nyholm, R., Trotman-Dickenson, A. F., Eds.; Pergamon: Oxford, U.K., 1973; Vol. 1, p 213. Seppelt, K.; Lentz, D. *Prog. Inorg. Chem.* **1982**, *29*, 167.

(10) (a) Hornbeck, J. A.; Molnar, J. P. *Phys. Rev.* **1951**, *84*, 621. Munson, M. S. B.; Franklin, J. L.; Field, F. H. *J. Phys. Chem.* **1963**, *67*, 1542. (b) Ng, C. Y.; Trevor, D. J.; Mahan, B. H.; Lee, Y. T. *J. Chem. Phys.* **1976**, *65*, 4327. (c) Dehmer, P. M.; Dehmer, J. L. *J. Chem. Phys.* **1977**, *67*, 1774; **1978**, *68*, 3462. (d) Jones, P. R.; Conklin, G. M.; Lorents, D. C.; Olson, R. E. *Phys. Rev. A* **1974**, *10*, 102. Mittmann, H.-U.; Weise, H.-P. *Z. Naturforsch.* **1974**, *29A*, 400.

(11) (a) Mulliken, R. S. *J. Chem. Phys.* **1970**, *52*, 5170; *Radiat. Res.* **1974**, *59*, 357. (b) Wadt, W. R. *J. Chem. Phys.* **1978**, *68*, 402. (c) Michels, H. H.; Hobbs, R. H.; Wright, L. A. *J. Chem. Phys.* **1978**, *69*, 5151; **1979**, *71*, 5053. (d) Ermler, W. C.; Lee, Y. S.; Pitzer, K. S.; Winter, N. W. *J. Chem. Phys.* **1978**, *69*, 976. Christiansen, P. A.; Pitzer, K. S.; Lee, Y. S.; Yates, J. H.; Ermler, W. C.; Winter, N. W. *J. Chem. Phys.* **1981**, *75*, 5410.

0020-1669/92/1331-5041$03.00/0

and despite its importance as an energy-absorbing species in xenon halide lasers (setting an upper limit to the xenon pressure which can be used),[12] there was no evidence prior to 1978[13] that the condensed phases could sustain more than transiently a species which is at once so acidic and weakly bound.

One of us noted[14] some years ago that when xenon reacts at room temperature with certain dioxygenyl salts, e.g. $O_2^+SbF_6^-$, a bright green color is initially imparted to the solid. As the noncomplementary redox reaction proceeds further, so the green color gives place to the pale yellow color characteristic of the ultimate solid product, $XeF^+Sb_2F_{11}^-$, formed in accordance with eq 2. Still earlier accounts of the chemistry of xenon difluoride

$$Xe + 2O_2^+SbF_6^- \rightarrow XeF^+Sb_2F_{11}^- + 2O_2 \quad (2)$$

also included several references to an evanescent green coloration.[15] We have found that a similar green color is produced irreversibly when $XeF^+Sb_2F_{11}^-$ dissolved in antimony pentafluoride interacts with a limited supply of water or a variety of other reducing agents.[13] Moreover, the color persists indefinitely under these conditions at ambient temperatures provided that the solution is maintained under a positive pressure of xenon gas. The color is discharged with the removal of the xenon but returns with its reintroduction, the intensity varying with the gas pressure.[16,17] This process can be repeated many times and is highly reproducible, implying that the antimony pentafluoride medium is host to a reversible reaction between xenon and $XeF^+Sb_2F_{11}^-$.

The green species can be tracked in three ways. First, it has a distinctive UV–visible spectrum with strong absorptions in the mid-UV and red regions giving a transparent window centered near 530 nm. Second, its appearance is associated with the growth of a characteristic ESR signal observed to best effect with the sample frozen to 4.5 or 77 K. Third, the green coloration is paralleled by the growth of a single Raman line at 123 cm^{-1}. Enrichment of xenon first in the isotope ^{136}Xe ($I = 0$) and then in ^{129}Xe ($I = {}^1/_2$)[18] produces significant changes in the ESR spectrum affirming that the carrier of the paramagnetism is the dixenon(1+) cation, Xe_2^+. Resonance Raman studies, quantitative measurements of intensity versus xenon overpressure, and comparisons with the properties exhibited not only by the isoelectronic species I_2^- but also by Xe_2^+ as modeled by ab initio calculations[11] all lead to the inference that Xe_2^+ is the unique source of all the spectroscopic signals that go with the green coloration. The intensity measurements can be reconciled with the reversible formation of Xe_2^+ in accordance with the equilibrium (3), but the dependence of the visible absorbance on the $XeF^+Sb_2F_{11}^-$ concentration implies a secondary equilibrium (4) affording a complex incorporating Xe_2^+ and an excess of the oxidant.[16]

$$3Xe + XeF^+Sb_2F_{11}^- + 2SbF_5 \rightleftarrows 2Xe_2^+Sb_2F_{11}^- \quad (3)$$

$$Xe_2^+Sb_2F_{11}^- + XeF^+Sb_2F_{11}^- \rightleftarrows Xe_2^+Sb_2F_{11}^-\cdot XeF^+Sb_2F_{11}^- \quad (4)$$

This paper presents a full account of the results and arguments underlying these conclusions and establishing Xe_2^+ as the first binuclear noble gas cation to show a significant presence in the condensed phases. The studies go back more than 15 years, and preliminary accounts of various aspects were published some years ago;[13,16] findings hitherto unpublished were outlined at a recent conference[19] and featured in graduate or doctoral dissertations.[20] How Xe_2^+ came to be identified has also been described in brief as a case history illustrating the use of spectroscopic methods in inorganic chemistry.[21]

Results and Discussion

(i) Formation of the Green Coloration. With antimony pentafluoride as the reaction medium, liquid samples with a green coloration long-lived at ambient temperatures can be prepared in one of three ways. (a) Elemental xenon reacts with the dioxygenyl salt $O_2^+Sb_2F_{11}^-$ largely in accordance with eq 5, but

$$Xe + 2O_2^+Sb_2F_{11}^- \rightarrow XeF^+Sb_2F_{11}^-\cdot 2SbF_5 + 2O_2 \quad (5)$$

an excess of xenon imparts a distinct green color to the otherwise pale yellow product. This route is important as it affords the most convenient and economical way of varying the isotopic composition of the green species. (b) The xenon(II) salt $XeF^+Sb_2F_{11}^-$ is reduced irreversibly with a deficiency of a suitable reducing agent; the green coloration persists for as long as a positive pressure of xenon is maintained over the product. The following reductants have been found to function in this way: a metal like lead or mercury, water, SO_2, PF_3, SbF_3, CO, PbO, As_2O_3, finely divided silica, and glass wool. (c) The reversible reaction of elemental xenon with $XeF^+Sb_2F_{11}^-$ gives the cleanest and most easily controlled route to the green product. In all probability, methods a and c do not differ in the ultimate step giving rise to the green product, although some samples of this product prepared from $O_2^+Sb_2F_{11}^-$ have been shown by their ESR[22] and Raman[23] spectra to retain small amounts of the unchanged O_2^+ cation. The similarity of the first ionization potentials of xenon (12.13 eV)[18] and dioxygen (12.06 eV)[18] has prompted us to investigate whether the reaction of a dioxygenyl salt with elemental xenon is reversible, but detailed studies of $XeF^+Sb_2F_{11}^-$ under various pressures of dioxygen have failed to detect any sign suggesting the formation of the O_2^+ cation.[22,23] Although method b was used in many of the earlier studies, it has several disadvantages. Since elemental xenon is also a product of the partial reduction of $XeF^+Sb_2F_{11}^-$, it is difficult to assess the roles of this and of the primary reductant as immediate precursors to the green product. The intensity of the coloration initially developed does not, however, correlate with the pressure of elemental xenon released, and so it seems that both reversible and irreversible routes gives access to the green product. Moreover, side reactions cannot necessarily be discounted, and the oxidized form of the reductant—whose identity is not always certain—is another potential source of confusion. We have therefore relied latterly on methods a and c for definitive information about the green product.

(12) Champagne, L. F.; Harris, N. W. *Appl. Phys. Lett.* **1977**, *31*, 513. Hawryluk, A. M.; Mangano, J. A.; Jacob, J. H. *Appl. Phys. Lett.* **1977**, *31*, 164.
(13) Stein, L.; Norris, J. R.; Downs, A. J.; Minihan, A. R. *J. Chem. Soc., Chem. Commun.* **1978**, 502.
(14) Stein, L. *Nature* **1973**, *243*, 30.
(15) Cohen, B.; Peacock, R. D. *J. Inorg. Nucl. Chem.* **1966**, *28*, 3056. Edwards, A. J.; Holloway, J. H.; Peacock, R. D. *Proc. Chem. Soc.* **1963**, 275. Holloway, J. H.; Knowles, J. G. *J. Chem. Soc. A* **1969**, 756.
(16) Stein, L.; Henderson, W. W. *J. Am. Chem. Soc.* **1980**, *102*, 2856.
(17) An illustration showing the green coloration is given in: Holloway, J. H. *J. Fluorine Chem.* **1986**, *33*, 150.
(18) *CRC Handbook of Chemistry and Physics*, 72nd ed.; CRC Press: Boca Raton, FL, 1991–1992.
(19) Brown, D. R.; Clegg, M. J.; Downs, A. J.; Fowler, R. C.; Minihan, A. R.; Stein, L. 13th International Symposium on Fluorine Chemistry, Ruhr-Universität Bochum, Germany, Sept 1991; *J. Fluorine Chem.* **1991**, *54*, 396.
(20) Miniham, A. R. D.Phil. Thesis, University of Oxford, 1981. Fowler, R. C. Part II Thesis, University of Oxford, 1981. Clegg, M. J. Part II Thesis, University of Oxford, 1986. Brown, D. R. Part II Thesis, University of Oxford, 1991.
(21) Ebsworth, E. A. V.; Rankin, D. W. H.; Cradock, S. *Structural Methods in Inorganic Chemistry*, 2nd ed.; Blackwell Scientific Publications: Oxford, U.K., 1991; p 401.
(22) (a) Shamir, J.; Binenboym, J. *Inorg. Chim. Acta* **1968**, *2*, 37. (b) Goldberg, I. B.; Christe, K. O.; Wilson, R. D. *Inorg. Chem.* **1975**, *14*, 152.
(23) Griffiths, J. E.; Sunder, W. A.; Falconer, W. E. *Spectrochim. Acta, Part A* **1975**, *31*, 1207.

The ability of water, finely divided silica, and glass wool to reduce $XeF^+Sb_2F_{11}^-$ and so act as sources of the green product emphasizes the potential importance of both the materials used for containment and their condition. Most of the experiments described here were carried out in Pyrex glass or quartz apparatus. Provided that this had been passivated beforehand by heating under continuous pumping and exposure to elemental fluorine, it gave reproducible results for the growth and decay of the green coloration in the reversible reaction of elemental xenon with $XeF^+Sb_2F_{11}^-$, and samples of the green antimony pentafluoride liquor could be kept in such apparatus at room temperature for months at a time with little or no diminution in the intensity of the coloration. Experiments with apparatus made in prepassivated metal, PTFE, and Teflon-FEP gave similar results albeit, typically, of inferior spectroscopic quality. It seems reasonable therefore to assume that the substance of what is reported here is a function neither of the material used for the fabrication of the apparatus nor of the intervention of moisture or other adventitious impurities. On the other hand, most of the earlier sightings of green colorations[15] are likely to have had their origins in traces of moisture or other oxidizable impurities resulting from the use of imperfectly passivated apparatus; it is surely significant that green colorations do not feature in reports of later studies employing rigorously conditioned apparatus.[24,25]

One other impurity is liable to affect the reactivity of $XeF^+Sb_2F_{11}^-$, namely xenon(IV) traces of which may be present in the xenon difluoride used to prepare the XeF^+ salt. Antimony pentafluoride solutions then contain as an impurity the salt $XeF_3^+Sb_2F_{11}^-$,[26] which inhibits the formation of the green color through its preferential reaction with elemental xenon to form the XeF^+ cation (eq 6). For quantitative studies aimed at determining the stoichiometry of the reaction between xenon and $XeF^+Sb_2F_{11}^-$, it is imperative therefore to use pure samples of the XeF^+ salt free from contamination by xenon(IV).

$$Xe + XeF_3^+Sb_2F_{11}^- + 2SbF_5 \rightarrow 2XeF^+Sb_2F_{11}^- \quad (6)$$

Antimony pentafluoride is far from ideal as a reaction medium. Its viscosity at normal temperatures is comparable with that of glycerol and some 400–500 times that of water,[27] and despite its unusual acidity, its minimal response to acidic centers makes it but a poor solvent for ionic solids. The salt $XeF^+Sb_2F_{11}^-$ is not freely soluble in antimony pentafluoride but, under equilibrium conditions, separates into two liquid phases, one rich in the salt and the other rich in antimony pentafluoride. A single homogeneous liquid phase is formed only when the biphasic system is heated to temperatures in excess of 40 °C, although the propensity of the viscous material for supercooling means that the single phase will often persist metastably for some hours at room temperature. Numerous attempts have been made to find a more convenient and conventional host for the green product, with the results summarized in Table I. Thus, we note that addition of hydrogen fluoride to an antimony pentafluoride solution results in the evolution of xenon and progressive fading of the green color such that no perceptible coloration could be detected in mixtures with the composition $HF:SbF_5 >$ ca. 1:1, even at low temperatures. Fluorosulfonic acid proved no more satisfactory, with the added complication that it is oxidized by the XeF^+ salt to peroxodisulfuryl difluoride (eq 7).[28] Of the other pentafluorides tried—AsF_5, BrF_5, and IF_5—none showed useful solvent action

Table I. Results of Searches for Media Capable of Supporting the Green Intermediate Formed by the Reduction of XeF^+ Salts

medium	finding
SbF_5	green solutions stable at room temperature can be prepared
$HF–SbF_5$	green product unstable when $HF:SbF_5 >$ ca. 1:1
HSO_3F	reacts with XeF^+ and does not support the green product
AsF_5	only traces of green color detectable at low temperatures
BrF_5 and IF_5	do not support the green product

supporting the formation of the green product, although signs of a green coloration could sometimes be detected, as with the

$$XeF^+Sb_2F_{11}^- + 5HSO_3F \rightarrow Xe + S_2O_6F_2 + HF + SbF_6^- + SbF_5(SO_3F)^- + 2H_2SO_3F^+ \quad (7)$$

reaction between xenon and $O_2^+AsF_6^-$. There is still some scope for extending this search, but the evidence accumulated to date suggests that the survival of the green product in significant concentrations at ambient temperatures is peculiar to antimony pentafluoride as a medium.

Numerous experiments have also been carried out in an attempt to isolate the green product free from any solid or liquid support. Most formidable of the various obstacles to be overcome are the following: (a) The product shows no sign of being volatile under normal conditions. (b) Antimony pentafluoride, the only liquid medium known to support it in appreciable concentration, is viscous and relatively involatile and high-melting. (c) The degree of formation of the product from $XeF^+Sb_2F_{11}^-$ is invariably small under equilibrium conditions (q.v.). (d) Irreversible reduction of an XeF^+ salt to achieve a higher (nonequilibrium) concentration of the product is handicapped by the factors common to this approach (q.v.) and by the aggravated problems of separation which it usually implies. The reversible route appears to offer little prospect of isolating the product, and so we have concentrated mainly on irreversible routes. The best hope seems to lie with a reductant like SO_2 or CO, which is oxidized to a volatile, relatively inert product, or with one like SbF_3, which is oxidized to a constituent (SbF_5) of the primary reaction mixture. Experiments with SO_2, CO, and PF_3 have failed to give the green product in concentrations exceeding those which can be achieved by reversible means, probably because the appropriate irreversible reactions are slower than the reversible one. By contrast, the reaction of XeF_2 with SbF_3 in the presence of SbF_5 is capable of yielding in a closed system a solid so intensely colored as to appear almost black, but the product is not homogeneous and appears to be intractable to normal workup procedures.

In the absence of a support-free sample of the green product, we have had to depend on the spectroscopic properties of liquid and solid samples incorporating it to determine its identity, physical properties, and exact chemical provenance. Such a sample typically exhibits characteristic ESR, UV–visible, and Raman spectra; the details of each of these will be described and analyzed in turn in the following sections. Critical to the analysis are the answers which must also be found to the following questions. *How many and what species* are responsible for each of the various spectroscopic signals which correlate with the appearance of the green coloration? Can we be sure, moreover, that the species responsible for one type of signal is the *same* as that giving rise to another type of signal? The circumstances of the experiments give persuasive grounds for believing that we are dealing with a derivative of xenon in a formal oxidation state between 0 and +2. Possible identities for the product therefore include XeF, Xe_2F, Xe^+, Xe_2^+, Xe_2F^+, or something along these lines with three or more xenon atoms, but the antimony pentafluoride and perfluoroantimonate(V) anions may also have a significant part to play.

(24) Gillespie, R. J.; Landa, B. *Inorg. Chem.* **1973**, *12*, 1383.
(25) Gillespie, R. J.; Netzer, A.; Schrobilgen, G. J. *Inorg. Chem.* **1974**, *13*, 1455. Wechsberg, M.; Bulliner, P. A.; Sladky, F. O.; Mews, R.; Bartlett, N. *Inorg. Chem.* **1972**, *11*, 3063.
(26) Selig, H.; Holloway, J. H. *Top. Curr. Chem.* **1984**, *124*, 59.
(27) Woolf, A. A.; Greenwood, N. N. *J. Chem. Soc.* **1950**, 2200. Hoffman, C. J.; Jolly, W. L. *J. Phys. Chem.* **1957**, *61*, 1574.
(28) Symons, M. C. R. *J. Chem. Soc. A* **1971**, 2393. Mishra, S. P.; Symons, M. C. R.; Christe, K. O.; Wilson, R. D.; Wagner, R. I. *Inorg. Chem.* **1975**, *14*, 1103.

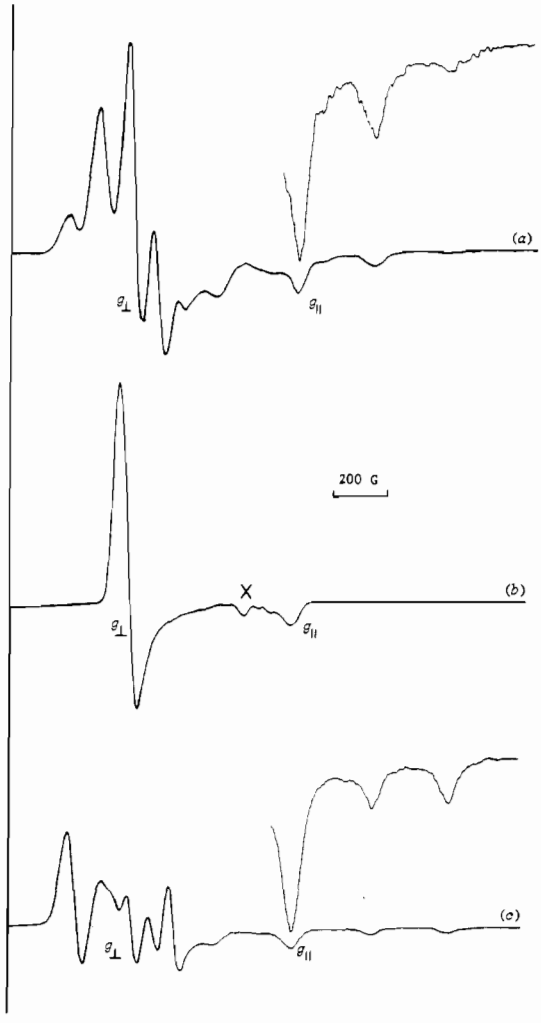

Figure 1. First derivative X-band ESR spectra displayed by samples of the green product formed by partial reduction of $XeF^+Sb_2F_{11}^-$ in a frozen SbF_5 matrix showing the effects of different isotopic compositions of xenon: (a) Isotopically natural xenon, sample at 4.5 K, with the insert showing the high-field region at increased gain; (b) ^{136}Xe, sample at 4.5 K, where X denotes resonance due to traces of O_2^+; (c) xenon enriched in ^{129}Xe (see Table II), sample at 77 K, with the insert showing the high-field region at increased gain.

(ii) ESR Spectra. We consider first the ESR spectra associated with the green product and measured at X- and Q-band frequencies. Through isotopic enrichment of the sample these admit a virtually unambiguous identification of the paramagnetic center. With all the reagents in their natural isotopic forms, a sample of the green product generated from $XeF^+Sb_2F_{11}^-$ in antimony pentafluoride and frozen at 4.5 K gives the well-defined ESR spectrum illustrated in Figure 1a; this spectrum is wholly reproducible and does not change with the method of preparation (i.e. whether method a, b, or c). Qualitative studies suggest that the intensity of the ESR signal correlates with that of the green coloration. The relative richness of structure implies hyperfine coupling to one or more magnetic nuclei. Nuclei known to be present and which may be implicated in such coupling include ^{19}F ($I = {}^1/_2$, 100%), ^{121}Sb ($I = {}^5/_2$, 57.4%), ^{123}Sb ($I = {}^7/_2$, 42.6%), ^{129}Xe ($I = {}^1/_2$, 26.4%), and ^{131}Xe ($I = {}^3/_2$, 21.2%), the appropriate spins and natural abundances being as listed in parentheses.[18]

(a) Isotopically Enriched Samples. To determine the origin of the coupling, a sample of the green product has been prepared from $O_2^+Sb_2F_{11}^-$ and ^{136}Xe for which $I = 0$,[18] and the resulting ESR spectrum of a frozen antimony pentafluoride solution is as shown in Figure 1b. The marked simplification brought about in this way leaves no doubt that xenon nuclei are responsible for the hyperfine splitting in the spectrum of the natural product and so affirms that xenon is an ingredient of the paramagnetic center. Of hyperfine interactions implicating any other nucleus, e.g. ^{19}F, ^{121}Sb, and ^{123}Sb, at least with $A >$ ca. 10 G, there is no vestige. Since the $A(^{19}F)$ values for the radicals XeF and Kr_2F are 180–960[7a] and 280–1180 G,[7d] respectively, and the $A(^{121}Sb)$ values for various fluoroantimony radicals are 30–70 G,[28] it is highly unlikely that the paramagnetic center associated with the green color embraces either fluorine or antimony. Instead the spectrum we observe for the product formed by ^{136}Xe displays not hyperfine splitting but the simple "powder" pattern characteristic of a set of randomly oriented radicals each with $S = {}^1/_2$ and an axially symmetric but highly anisotropic g tensor.[29] Hence the principal values of the g tensor can be extracted giving $g_\parallel = 1.885$ and $g_\perp = 2.304$. The logical inference of these findings is that we are dealing with a radical composed *exclusively* of xenon. The most likely candidates are Xe^+, Xe_2^+, and Xe_3^+ (either linear or in the form of an isosceles triangle). The next step is to refer back to the product formed from isotopically natural xenon in order to determine which of these candidates gives the best account of the hyperfine splitting.

The statistical distribution of the magnetic isotopes ^{129}Xe and ^{131}Xe leads to the following numbers of different possible spin-systems: Xe^+, 3; Xe_2^+, 6; Xe_3^+, 10. For a given radical each spin-system is associated with a different splitting pattern, and these patterns will all be superimposed in a first-order ESR spectrum (see Table II). The magnetogyric ratios of ^{129}Xe and ^{131}Xe are such[18] that $A(^{129}Xe) = -3.37A(^{131}Xe)$, and accordingly the splitting pattern as a whole is expected to be dominated by coupling to ^{129}Xe. The spectrum of Xe^+ should therefore approximate to a triplet pattern with components having relative intensities in the order of 1:5:1, that of Xe_2^+ to a quintet pattern with relative intensities of roughly 1:11:30:11:1, and that of Xe_3^+ also to a quintet pattern but now with relative intensities of roughly 1:5:10:5:1. In the event, the spectrum displayed by the green product formed by xenon of natural isotopic composition shows an unmistakable quintet pattern for the more intense perpendicular component, and the high-field line of a similar pattern is just discernible in the weaker and partially overlapping parallel component (see Figure 2a). There is no question therefore but that Xe^+ can be dismissed as the carrier of the signal. As between the other two options there is less to choose, but the intensities of the lines observed in the parallel region match the predictions for Xe_2^+ more closely than those for Xe_3^+. Indeed the spectrum expected for Xe_2^+ can be calculated in first order on the basis of the natural abundances of the spin-active xenon isotopes, the g values measured in the experiment with ^{136}Xe, and of A values optimized to give the best account of the measured spectrum. The result, as illustrated in Figure 2b and based on the parameters $g_\perp = 2.304$, $g_\parallel = 1.885$, $A_\perp(^{129}Xe) = 220$ G, $A_\perp(^{131}Xe) = 65.2$ G, $A_\parallel(^{129}Xe) = 600$ G, and $A_\parallel(^{131}Xe) = 178$ G,[13] reproduces remarkably well the main features of the measured spectrum (Figure 2a). By contrast, the corresponding spectrum calculated for Xe_3^+ (Figure 2c) fits the measured spectrum rather less closely. Even with Xe_2^+ the fit is not perfect, and it is evident both from the measured spectrum and from the magnitudes of the ESR parameters that significant second-order effects are at work, particularly in the $g_\perp$ region of the spectrum where the hyperfine lines are seen to be unequally spaced.

To check these conclusions, a sample of the green product has been prepared from $O_2^+Sb_2F_{11}^-$ and xenon enriched in the spin-$^1/_2$ nucleus ^{129}Xe (^{129}Xe, 80.3%; ^{131}Xe, 3.8%; and nonspinning isotopes $^*Xe$, 15.9%), and its X-band ESR spectrum recorded, with the results illustrated in Figure 1c. On the assumption that Xe_2^+ is the carrier of the ESR signal, the main contribution to the spectrum now comes from just two isotopomers, viz. $^{129}Xe_2^+$ (64.5%), which is expected to give rise to a 1:2:1 triplet, and $^{129}Xe^*Xe^+$ (25.5%), which should give a doublet (Table II). The

(29) Kneubühl, F. K. *J. Chem. Phys.* **1960**, *33*, 1074.

Table II. Different Isotopomers of the Species Xe_n^+ (n = 1–3): Abundances and ESR Hyperfine Splitting Patterns in First-Order Spectra

			abundance (%)	
n	isotopomer[a]	ESR hyperfine splitting pattern	naturally occurring Xe[b]	^{129}Xe-enriched sample[c]
1	^{129}Xe	doublet	26.4	80.3
	^{131}Xe	1:1:1:1 quartet	21.2	3.8
	*Xe	singlet	52.4	15.9
2	^{129}Xe^{129}Xe	1:2:1 triplet	7.0	64.5
	^{129}Xe^{131}Xe	doublet of 1:1:1:1 quartets	11.2	6.1
	^{129}Xe*Xe	doublet	27.7	25.5
	^{131}Xe^{131}Xe	1:2:3:4:3:2:1 septet	4.5	0.1
	^{131}Xe*Xe	1:1:1:1 quartet	22.2	1.2
	*Xe*Xe	singlet	27.5	2.5
3	^{129}Xe^{129}Xe^{129}Xe	1:3:3:1 quartet	1.8	51.8
	^{129}Xe^{129}Xe^{131}Xe	triplet of 1:1:1:1 quartets	4.4	7.4
	^{129}Xe^{129}Xe*Xe	1:2:1 triplet	11.0	30.8
	^{129}Xe^{131}Xe^{131}Xe	doublet of 1:2:3:4:3:2:1 septets	3.6	0.3
	^{129}Xe^{131}Xe*Xe	doublet of 1:1:1:1 quartets	17.6	2.9
	^{129}Xe*Xe*Xe	doublet	21.7	6.1
	^{131}Xe^{131}Xe^{131}Xe	decet	1.0	0.0
	^{131}Xe^{131}Xe*Xe	1:2:3:4:3:2:1 septet	7.1	0.1
	^{131}Xe*Xe*Xe	1:1:1:1 quartet	17.5	0.3
	*Xe*Xe*Xe	singlet	14.4	0.4

[a] *Xe represents all nonspinning Xe isotopes. [b] See ref 18. [c] Based on composition specified by the supplier (see Experimental Section).

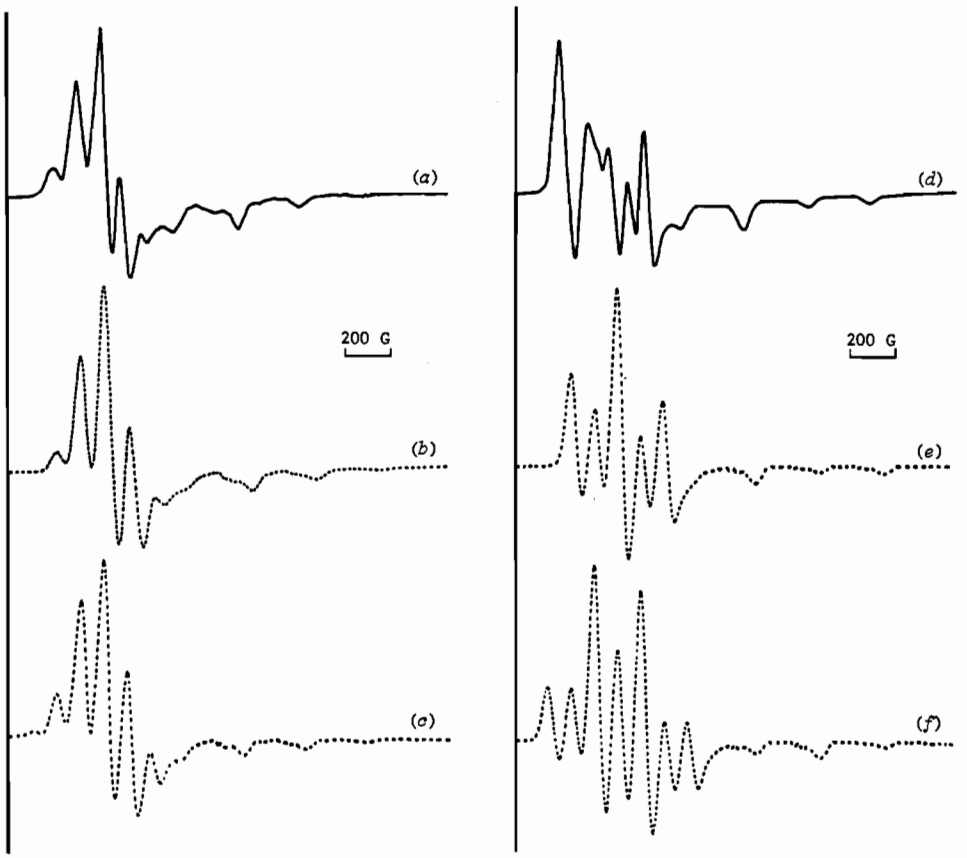

Figure 2. Comparison of the measured X-band ESR spectra of the green product with those simulated in first order for the species Xe_2^+ or Xe_3^+ characterized by the following parameters: $g_\perp$ = 2.304, $g_\parallel$ = 1.885; $A_\perp(^{129}Xe)$ = 220, $A_\perp(^{131}Xe)$ = 65.2, $A_\parallel(^{129}Xe)$ = 600, and $A_\parallel(^{131}Xe)$ = 178 G. Sample prepared from isotopically natural xenon: (a) observed spectrum; (b) spectrum calculated for Xe_2^+; (c) spectrum calculated for Xe_3^+. Sample prepared from ^{129}Xe-enriched xenon: (d) observed spectrum; (e) spectrum calculated for Xe_2^+; (f) spectrum calculated for Xe_3^+.

overall result should be a quintet with components having intensities in the order of 1:1:2.3:1:1. Were Xe_3^+ the carrier, the relatively large contribution made by $^{129}Xe_3^+$ (51.8%) would cause the splitting pattern to appear *not* as a quintet but as a septet with components having intensities roughly in the ratios 1:1.5:3.7:3.0:3.7:1.5:1. Any remaining doubts about the identity of the paramagnetic center are eliminated by the measured spectrum, the $g_\parallel$ portion of which, while overlapping partly, and being perturbed by, the $g_\perp$ portion, reveals four of the five lines with the relative intensities predicted for Xe_2^+; such a pattern cannot be reconciled with Xe_3^+. This point is reinforced by simulations of the spectra, as in Figure 2e,f, but the limitations of the first-order approximation are now much more exposed, with the intensity pattern, spacing, and other details of the $g_\perp$ component departing significantly from the simple five-line pattern suggested by the calculations. We have sought to overcome these complications in two ways, namely by measuring the Q-band spectra or by calculating the spectra in second order.

(b) Q-Band Measurements. We have measured the ESR spectra of samples of the green product in antimony pentafluoride frozen at ca. 99 K under Q-band conditions (with an operating frequency of 34 098 MHz, as opposed to ca. 9000 MHz for the

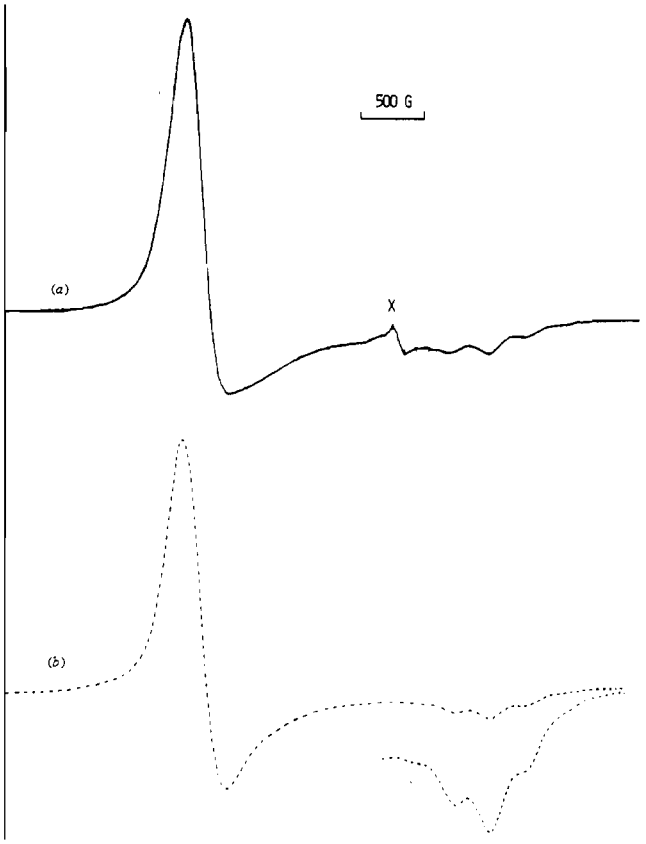

Figure 3. First derivative Q-band ESR spectra (a) measured for a sample of the green product prepared from isotopically natural xenon and frozen in an SbF_5 matrix at ca. 99 K (X denotes resonance due to traces of O_2^+) and (b) calculated for Xe_2^+. The calculations were at second-order level and assumed a Lorentzian line shape with a width-at-half-height of 150 G, together with the following parameters: $g_\perp = 2.312$, $g_\parallel = 1.888$; $A_\perp(^{129}Xe) = 200$, $A_\perp(^{131}Xe) = 60$, $A_\parallel(^{129}Xe) = 620$, and $A_\parallel(^{131}Xe) = 185$ G.

X-band measurements). However, instead of producing a clearer separation of the parallel and perpendicular components and improved and simplified definition of the hyperfine structure, the results showed only an intense, broad resonance for $g_\perp$ with no clearly discernible hyperfine splitting, together with a $g_\parallel$ component similar in form to, but relatively much weaker than, that observed in the corresponding X-band spectra (see, for example, Figure 3). Moreover, the large increase in line width occasioned by the switch from X-band to Q-band excitation did not, as might have been hoped, decrease significantly when the sample was diluted. These findings lead us to believe that a major contribution to the line width of the ESR signal comes from so-called "*g*-strain" effects arising from small variations in local site geometry in the solid amorphous sample which result in a distribution of *g* and *A* values if the corresponding tensors are relatively anisotropic.[30] Precedents for these effects are to be found, for example, in the ESR spectra of various copper(II) compounds which have been analyzed in some detail.[31] Hence the formula in eq 8 has been derived linking the width-at-half-height for the $g_\parallel$ resonance, $\Delta B_{1/2}$, to the resonant frequency ν_0 and the nuclear spin quantum number m_I, where $\Delta B^R_{1/2}$ is the residual line width in the absence of strain, $\sigma_{g_\parallel}$ and $\sigma_{A_\parallel}$ are the widths at half-amplitude of the Gaussian distributions of $g_\parallel$ and $A_\parallel$, respectively, μ is the Bohr magneton, and ϵ is the correlation coefficient between $\sigma_{g_\parallel}$ and $\sigma_{A_\parallel}$. If formula (8) is generally valid, the line width may be

$$(\Delta B_{1/2})^2 = (\Delta B^R_{1/2})^2 + (m_I\sigma_A)^2 + \left(\frac{h\nu_0}{g_\parallel^2\mu}\sigma_{g_\parallel}\right)^2 + \epsilon\left(\frac{2m_I h\nu_0}{g_\parallel^2\mu}\right)\sigma_{g_\parallel}\sigma_{A_\parallel} \quad (8)$$

expected typically to increase at higher microwave frequencies ν_0, to the detriment of the spectral resolution. Herein, we believe, lies the most plausible explanation for the large line widths which characterized the Q-band spectra. When *g*-strain is operative, however, the line width depends also on m_I and, for certain m_I values, does not change monotonically but goes to a minimum, as ν_0 varies. This m_I-dependence of the line width provides a basis for rationalizing some of the finer details of the X-band spectra which elude simulation.

(c) Second-Order Calculations. Since Q-band measurements failed to give any new information, we have carried out more sophisticated calculations of the ESR spectra with the aid of a program taking account of second-order effects.[32] In this way, for example, the Q-band spectrum illustrated in Figure 3a could be satisfactorily matched on the assumption of a Lorentzian (rather than a Gaussian) line shape with a width-at-half-height of 150 G (see Figure 3b). The results of similar calculations of the X-band spectra associated with isotopically natural Xe_2^+ and Xe_3^+ are illustrated in Figure 4; in this case a Gaussian line shape with a width of 50 G appears to give the best account of the experimental findings. Hence, it is apparent that a very close approximation to the measured spectrum is provided by Xe_2^+ but not by Xe_3^+. Moreover, the simulation now reproduces not only the intensity pattern of this spectrum but also the unequal splittings between the five major perpendicular lines (120, 120, 100, and 100 G in order of increasing field), a feature outside the scope of the first-order calculations. The only significant difference between the experimental and calculated spectra is that the features at lowest field appear slightly better resolved in the latter suggesting that, in practice, the line width increases somewhat at lower field.

By contrast, the X-band spectrum of the product enriched in ^{129}Xe proves to be a more searching test of the calculations because the isotopomer $^{129}Xe_2^+$ now accounts for nearly two-thirds of the total intensity. The best simulation, illustrated in Figure 4, offers a major improvement on the first-order calculations in its replication of the main features in the overall intensity pattern displayed by the measured spectrum. As before, the measured spectrum differs from the calculated one in the increasing line width of the perpendicular lines at low field. A more obvious discrepancy is the splitting of the central perpendicular line associated with the $I = 1$, $m_I = 0$ and $I = 0$, $m_I = 0$ components. The second-order calculations correctly anticipate this splitting but with a magnitude of ca. 50 G, yet the splitting in the measured spectrum *appears* to be about twice as big as this, with the result that the shifted component (due to $I = 1$, $m_I = 0$) overlaps the adjacent line to low field (see Figure 4). We have considered various possible causes of this anomaly, for example third-order effects, the intervention of "forbidden" transitions, etc., but the only one carrying any conviction comes back to *g*-strain and the associated line width variation already noted. Qualitative and semiquantitative analysis[33] based on eq 8 confirms the plausibility of such an explanation. Accordingly we believe that the line width variations and the superficially anomalous splitting of the central perpendicular line are both artifacts of *g*-strain.

Table III summarizes what appear to be the optimum ESR parameters for Xe_2^+ in a frozen antimony pentafluoride matrix at low temperatures. On the basis of these values and of the

(30) See, for example, the following: Anderson, R. E.; Durham, W. R.; Sands, R. H.; Bearden, A. J.; Crespi, H. L. *Biochim. Biophys. Acta* **1975**, *408*, 306. Pilbow, J. R. *Transition Ion Electron Paramagnetic Resonance*; Clarendon Press: Oxford, U.K., 1990; p 211.
(31) Froncisz, W.; Hyde, J. S. *J. Chem. Phys.* **1980**, *73*, 3123. Hyde, J. S.; Froncisz, W. *Annu. Rev. Biophys. Bioeng.* **1982**, *11*, 391.
(32) Program SIM: Lozos, G.; Hoffman, B.; Franz, C. Chemistry Department, Northwestern University.
(33) Clegg, M. J. Unpublished results.

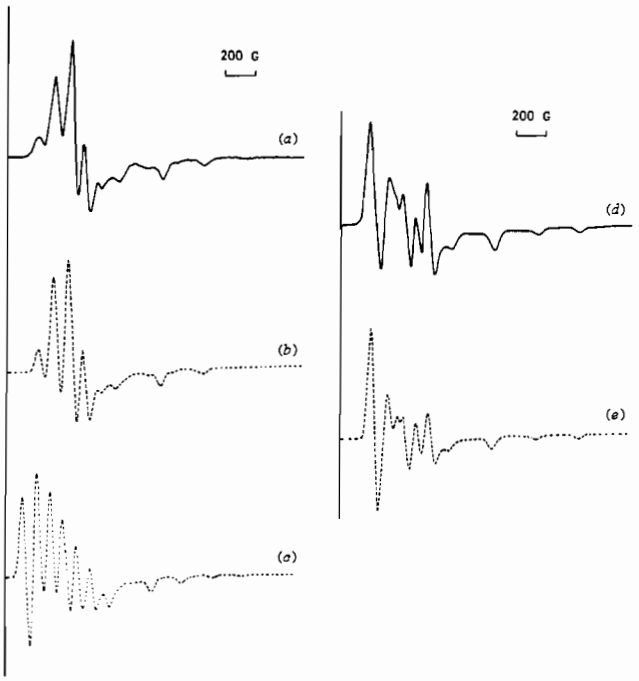

Figure 4. Comparison of the measured X-band ESR spectra of the green product with those simulated in second order for the species Xe_2^+ or Xe_3^+. The ESR signals were assumed to have Gaussian line shapes with a width-at-half-height of 50 G and to be characterized by the following parameters: $g_\perp = 2.312$, $g_\parallel = 1.888$; $A_\perp(^{129}Xe) = 200$, $A_\perp(^{131}Xe) = 60$, $A_\parallel(^{129}Xe) = 620$, and $A_\parallel(^{131}Xe) = 185$ G. Sample prepared from isotopically natural xenon: (a) observed spectrum; (b) spectrum calculated for Xe_2^+; (c) spectrum calculated for Xe_3^+. Sample prepared from ^{129}Xe-enriched xenon: (d) observed spectrum; (e) spectrum calculated for Xe_2^+.

Table III. ESR Parameters and Calculated Spin Densities for the Radicals Xe_2^+ and I_2^-

param	Xe_2^+ [a]	I_2^- [b]
g-tensor	$g_\parallel = 1.888$	$g_\parallel = 1.975, 1.975$
	$g_\perp = 2.312$	$g_\perp = 2.17, 2.175$
hyperfine tensor, A and B/G (MHz)	$A_\parallel(^{129}Xe) = 620\ (1640)$	$A_\parallel(^{127}I) = 405, 433$
	$A_\parallel(^{131}Xe) = 185\ (489)$	$A_\perp(^{127}I) = 115, 120$
	$A_\perp(^{129}Xe) = 200\ (650)$	
	$A_\perp(^{131}Xe) = 60\ (195)$	
	$A_{iso}(^{129}Xe) = 90\ (273)$ [c]	$A_{iso}(^{127}I) = 149, 151$ [c]
	$2B(^{129}Xe) = 449\ (1365)$ [c]	$2B(^{127}I) = 256, 280$ [c]
atomic parameters, A^0 and $2B^0$/G (MHz) [d]	$A^0(^{129}Xe) = 11\,785\ (33\,030)$	$A^0(^{127}I) = 7295$
	$2B^0(^{129}Xe) = 751\ (2105)$	$2B^0(^{127}I) = 453$
spin densities, a^2/%	$a^2_s = 0.8$ [e]	$a^2_s = 2.1, 2.1$
	$a^2_p = 60$ [e]	$a^2_p = 56, 61$

[a] Experimental results are for Xe_2^+ frozen with $XeF^+Sb_2F_{11}^-$ in an SbF_5 matrix at 77 or 4.5 K; g and A values are those giving the best account of the measured spectrum with due allowance for second-order effects (see text). [b] Experimental results are for a γ-irradiated aqueous solution of an alkali-metal iodide at 77 K; the two sets of values correspond to I_2^- in two distinct sites. See ref 35b. [c] Calculated by the method indicated in ref 35b. [d] See ref 34. [e] Calculated on the assumption that $A_\parallel$ and $A_\perp$ have the *same* sign, otherwise a^2_p is calculated to be >100%. In fact, our spectra verify this point as the intensities would be different if $A_\parallel$ and $A_\perp$ took opposite signs, with the perpendicular components increasing in intensity toward *higher* field rather than toward *lower* field, as was observed in practice (most noticeably in the X-band spectrum of the ^{129}Xe-enriched sample; see Figure 1c).

corresponding parameters for a free xenon atom,[34] spin densities have been calculated. The results are also included in Table III, together with the corresponding properties of a known species isoelectronic with Xe_2^+, viz. the diiodine(1–) anion, I_2^-, present in V_k centers in solid metal iodides[35a] or as generated in other media.[35b,c] The comparison of these two formally $^2\Sigma_u^+$ radicals emphasizes their kinship and the dominance of p-character in the bonding, even more marked in Xe_2^+ than in I_2^- in keeping with the greater 5s–5p AO separation in the noble gas atom.

(34) Symons, M. *Chemical and Biochemical Aspects of Electron-Spin Resonance Spectroscopy*; Wiley: New York, 1978; p 176.

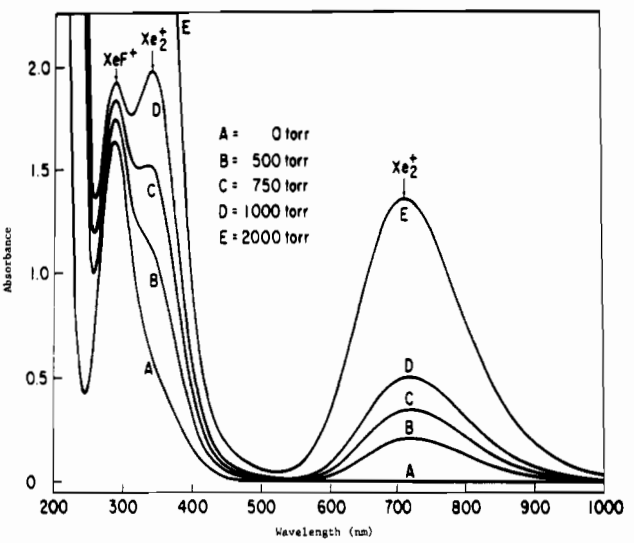

Figure 5. The UV–visible spectrum of an antimony pentafluoride solution of $XeF^+Sb_2F_{11}^-$ (0.404 mol dm^{-3}) at 25 °C showing the effects of different overpressures of xenon gas.

(iii) UV–Visible Absorption Spectrum. In the presence of xenon gas, an antimony pentafluoride solution containing $XeF^+Sb_2F_{11}^-$ develops two prominent UV–visible absorptions centered near 335 and 715 nm. The intensities of the absorptions vary with the overpressure of the xenon in the manner illustrated, for example, in Figure 5, and are found qualitatively to correlate with the intensity of the ESR signal. That the two optical absorptions are also due to Xe_2^+ is argued by the striking resemblance to the spectrum of the I_2^- anion, which, as formed in an alkali-metal iodide glass or a hydroxylic medium, likewise assumes a dark green color with strong absorptions at 370–400 and 737–800 nm.[35d] Equally persuasive is the closeness with which our results are matched by ab initio MO models for Xe_2^+.[11] With due allowance for spin–orbit coupling, such calculations impute to the two dipole-allowed electronic transitions highest in energy, $II(^1/_2)_g \leftarrow I(^1/_2)_u$ and $I(^1/_2)_g \leftarrow I(^1/_2)_u$, wavelengths of 340–375 and 740 nm, respectively.[11b,d] The calculations also identify a low-energy transition, $I(^3/_2)_g \leftarrow I(^1/_2)_u$, which should give rise to an absorption near 1200 nm but with an intensity at least 3 orders of magnitude lower than those of the higher-energy bands; attempts to detect this feature in practice have so far been unavailing.

Control experiments have shown that xenon dissolves in antimony pentafluoride to a limited extent and that, within the limits of experimental uncertainty, the solubility conforms to Henry's Law. As reported previously,[16] the absorbance of the band at 715 nm varies approximately as the $^3/_2$ power of the xenon pressure, a result in keeping with the stoichiometry of the equilibrium (3). Many subsequent measurements, made independently at both Argonne and Oxford, confirm not only the reversibility of the reaction between xenon and $XeF^+Sb_2F_{11}^-$ but also the dependence of the absorbance at 715 nm on the $^3/_2$ power of the xenon pressure (see, for example, Figure 6a). The UV band centered at 335 nm overlaps that centered at 287 nm due to $XeF^+Sb_2F_{11}^-$, but within the limits of uncertainty thus created, it matches the visible band in its behavior (see Figure 6b). That the absorbance of this band varies as marginally less than the $^3/_2$

(35) (a) Zvi, E. B.; Beaudet, R. A.; Wilmarth, W. K. *J. Chem. Phys.* **1969**, *51*, 4166. (b) Marov, I.; Symons, M. C. R. *J. Chem. Soc. A* **1971**, 201. (c) Shida, T.; Takahashi, Y.; Hatano, H.; Imamura, M. *Chem. Phys. Lett.* **1975**, *33*, 491. (d) Grossweiner, L. T.; Matheson, M. S. *J. Phys. Chem.* **1957**, *61*, 1089. Delbecq, C. J.; Hayes, W.; Yuster, P. H. *Phys. Rev.* **1961**, *121*, 1043. Fornier de Violet, P.; Bonneau, R.; Joussot-Dubien, J. *Chem. Phys. Lett.* **1973**, *19*, 251; **1974**, *28*, 569.

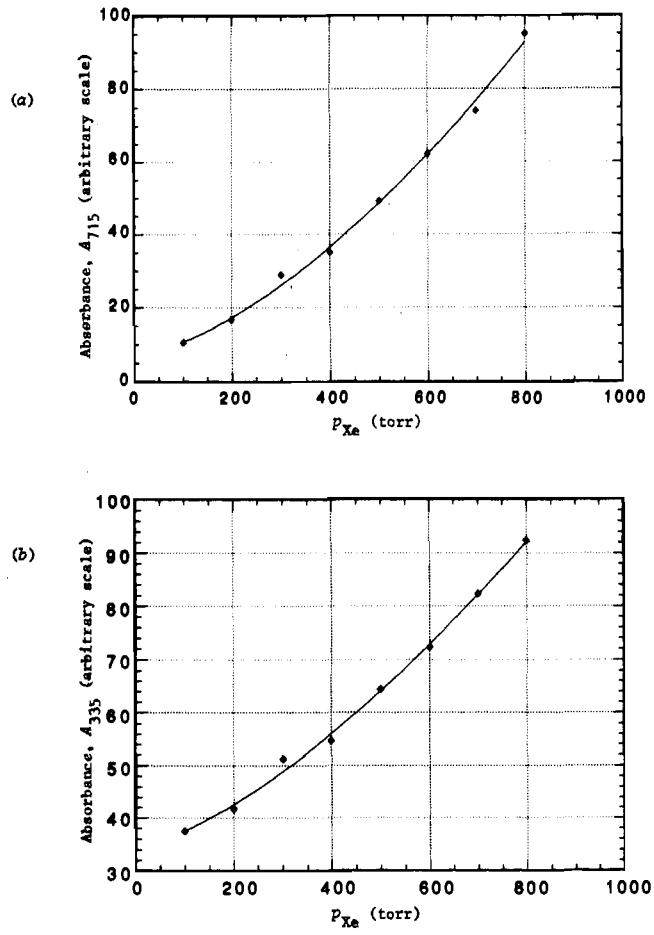

Figure 6. Best power regression curves linking the UV–visible absorbance (a) at 715 nm, A_{715}, and (b) at 335 nm, A_{335}, to the xenon overpressure, p_{Xe}. The results relate to an antimony pentafluoride solution ca. 0.4 mol dm^{-3} in $XeF^+Sb_2F_{11}^-$ and at 18 °C. For (a), $A_{715} = X + Yp_{Xe}^n$, where $n = 1.547$ with a correlation coefficient of 99.80%, and for (b), $A_{335} = X' + Y'p_{Xe}^n$, where $n = 1.420$ with a correlation coefficient of 99.83% (X, Y, X', and Y' are arbitrary constants).

power of the xenon pressure may signal some decay of the band at 287 nm with the buildup of the product presumed to be Xe_2^+; if so, the depletion in $XeF^+Sb_2F_{11}^-$ is quite small (<5% at a concentration of 0.4 mol dm^{-3}). On the other hand, there is no question but that the bands at 335 and 715 nm have a common source.

The effect of varying the concentration of $XeF^+Sb_2F_{11}^-$ has been described previously.[16] Hence, it emerges that the concentration of Xe_2^+, as measured by the absorbance of the 715-nm band, varies not as the square root of the $XeF^+Sb_2F_{11}^-$ concentration, as required by eq 3, but as the $^3/_2$ power of this concentration. Otherwise the concentration of Xe_2^+ is, as expected, proportional to the first power of the SbF_5 concentration. In order to explain these findings, it is necessary to invoke a second equilibrium (4) leading to a complex incorporating *both* Xe_2^+ and XeF^+, so that the overall reaction resulting from both electron transfer and complexation can be represented by eq 9. The spectral data yield a uniform equilibrium constant for this

$$3Xe + 3XeF^+Sb_2F_{11}^- + 2SbF_5 \rightleftarrows 2Xe_2^+Sb_2F_{11}^-\cdot XeF^+Sb_2F_{11}^- \quad (9)$$

reaction over a 16-fold range of xenon pressure and a 4-fold range of $XeF^+Sb_2F_{11}^-$ concentration, with the assumption of an arbitrary value for the molar extinction coefficient of the 715-nm band. As yet, however, it has not been possible to determine the extinction coefficient to arrive at an informed estimate of the equilibrium constant.

(iv) Raman Spectrum. The production of the green color, for example by the reversible reduction of $XeF^+Sb_2F_{11}^-$ by xenon in antimony pentafluoride solution, is accompanied by the appearance and growth of a polarized Raman line at 123 cm^{-1}. There is no other significant change in the Raman spectrum of the solution, the remaining bands being attributable to vibrational transitions of XeF^+,[24] $Sb_2F_{11}^-$,[24] and antimony pentafluoride.[36] The new line does not shift when the green product is made by different routes or when $H_2{}^{18}O$ supplants $H_2{}^{16}O$ as the reductant of $XeF^+Sb_2F_{11}^-$ (thereby tending to rule out the possibility of its originating in the vibration of a bond to oxygen). On the other hand, the replacement of the natural mixture of xenon isotopes by ^{136}Xe for the preparation of the green product reduces the wavenumber of the Raman band center by 2.4 ± 0.9 cm^{-1}. This is to be compared with a shift of 2.3 cm^{-1} calculated for Xe_2^+, although other species containing one or more Xe–Xe bonds, e.g. $XeXeF^+$ and Xe_3^+, would be expected to give a similar result.

Two series of experiments have been important in showing that the species responsible for the Raman emission at 123 cm^{-1} is also the carrier of the UV–visible bands at 335 and 715 nm and the ESR signal. One of these has involved systematic studies to determine how the intensity of the Raman line varies with the xenon overpressure. The other has exploited the resonance Raman effect to establish the link between the UV–visible bands and the Raman scattering.

(a) Intensity Measurements. The intensity measurements have been made with reference to the Raman spectrum excited at 514.5 nm, a wavelength close to the minimum in the UV–visible spectrum (see Figure 5) and deliberately chosen so as to minimize possible resonance Raman effects. The intensity of the Raman scattering at 123 cm^{-1} has been determined by measuring the area under the band and then normalizing it relative to the corresponding areas under the bands centered near 660 and 710 cm^{-1} due to $Sb_2F_{11}^-$ and the solvent, which appear to be invariant for a given concentration of $XeF^+Sb_2F_{11}^-$. Only by scrupulous attention to the avoidance of leaks, the elimination of impurities, and proper equilibration (through vigorous agitation of the sample) has it been possible to secure reproducible quantitative results. However, Figure 7 illustrates how, under appropriate conditions, the spectrum of a concentrated solution of $XeF^+Sb_2F_{11}^-$ in antimony pentafluoride (ca. 4 mol dm^{-3}) varies with the pressure of xenon gas admitted. The best computer-fitted power regression curve, shown in Figure 8, implies that the volume concentration of the species responsible for the Raman scattering at 123 cm^{-1} (as measured by the intensity of the signal) varies as the $^3/_2$ power of the xenon pressure. Similar measurements at different xenon pressures fail to show any significant change of intensity in the scattering at 619 cm^{-1} attributable to the XeF^+ cation.[24] Hence, it must be inferred that the new Raman signal at 123 cm^{-1}, like the UV–visible bands at 335 and 715 nm, is associated with the Xe_2^+ cation and that, once again, the percentage conversion of XeF^+ to Xe_2^+ is small and certainly less than 5%. Further studies show that, for a given xenon pressure, the intensity of the Raman scattering at 123 cm^{-1} increases monotonically with the $XeF^+Sb_2F_{11}^-$ concentration, but the weakness of the Raman effect has frustrated attempts to establish a quantitative relationship spanning an appreciable concentration range. ESR measurements made on a number of Raman samples also verify that the intensity of the resonance correlates, at least semiquantitatively, with the intensity of the Raman signal at 123 cm^{-1}.

(b) Resonance Raman Studies. That the electronic absorption bands at 335 and 715 nm and the Raman emission at 123 cm^{-1} come from the same species can also be affirmed by experiments in which the Raman spectrum is excited by radiation of different wavelengths, viz. 488.0, 514.5, 530.8, 568.2, 632.8, 647.1, and 676.4 nm. As the wavelength of the radiation moves progressively

(36) Beattie, I. R.; Livingston, K. M. S.; Ozin, G. A.; Reynolds, D. J. *J. Chem. Soc. A* **1969**, 958.

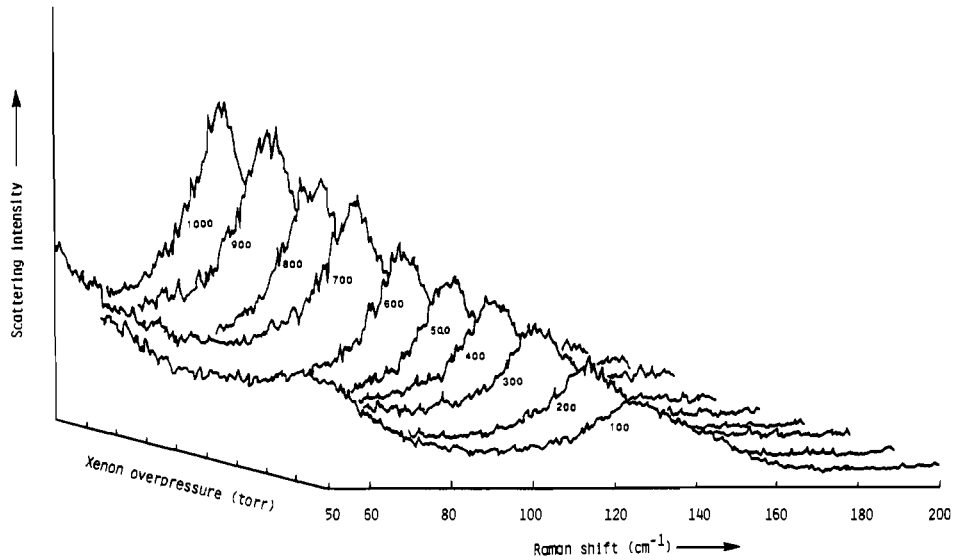

Figure 7. The low-frequency region of the Raman spectrum exhibited by a solution of $XeF^+Sb_2F_{11}^-$ in antimony pentafluoride (ca. 4 mol dm^{-3}) at 18 °C showing the effects of different overpressures of xenon gas.

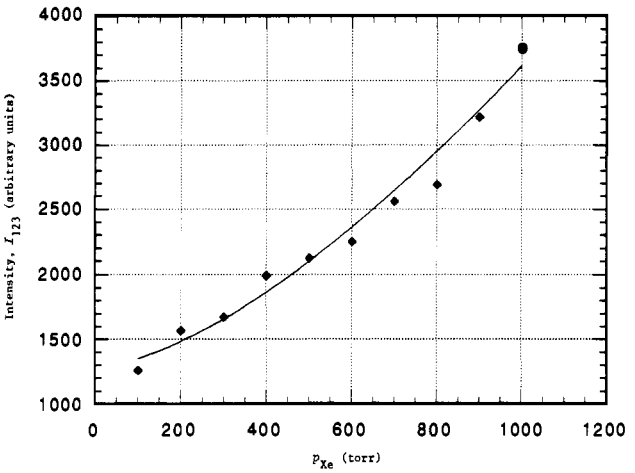

Figure 8. Best power regression curve linking the intensity of the Raman band at 123 cm^{-1}, I_{123}, to the xenon overpressure, p_{Xe}. The results relate to the spectra depicted in Figure 7. The curve corresponds to $I_{123} = X'' + Y''p_{Xe}^n$, where $n = 1.508$ and X'' and Y'' are arbitrary constants; the correlation coefficient is 98.73%.

into the envelope of the visible absorption band centered at 715 nm, so the Raman band at 123 cm^{-1} gains markedly in intensity with respect to those due to XeF^+, $Sb_2F_{11}^-$, and the solvent. In the limit set by excitation with radiation having $\lambda = 676.4$ nm, which lies close to the center of the electronic band, the spectrum is dominated by the Raman emission at 123 cm^{-1} and discloses, in addition, at least three overtones making up the kind of progression which is characteristic of a resonance Raman spectrum;[37] by contrast, the bands due to XeF^+, $Sb_2F_{11}^-$, and the solvent are barely discernible under these conditions (see Figure 9). The wavenumbers of the fundamental and first three overtones are as follows: ν 123 ± 0.5, 2ν 246 ± 5, 3ν 368 ± 11, and 4ν 480 ± 15 cm^{-1}. The marked increase of line width makes it impossible precisely to locate the centers of the overtone features, and so there is no question of being able to gain a useful estimate of the anharmonicity coefficient and hence an upper limit to the dissociation energy.[37] Freezing the sample to 77 K was found to cause some narrowing of the bands making up the resonance Raman progression (the half-widths being reduced to ca. 80% of those for the liquid sample at room temperature) but failed to improve significantly on the precision of the wavenumber measurements or to bring to light additional members of the progression. The broadness of the features is attributable partly to the spread of isotopic masses present in natural xenon (^{128}Xe to ^{136}Xe) and partly to the perturbation of a relatively strongly interacting environment. Unfortunately it has not yet been possible to carry out this sort of experiment with a sample of monoisotopic xenon, and there would clearly also be benefits from generating and trapping Xe_2^+ in a solid noble gas matrix at low temperatures. By contrast, the isoelectronic radical I_2^- has been generated in the form of matrix-isolated $M^+I_2^-$ ion pairs by cocondensation of alkali-metal atoms M with I_2 molecules and an excess of argon and characterized by resonance Raman measurements;[38] hence, the following parameters have been deduced: $\omega_e = 114.2$–115.6 cm^{-1}, $\omega_e x_e = 0.47$–0.50 cm^{-1}, and $D_e \leq 84$ kJ mol^{-1}. The vibrational properties thus evince once again the affinity of Xe_2^+ to I_2^-.

The limited range of wavelengths available for excitation of the Raman spectrum meant that it has not been feasible to chart a useful excitation profile taking in one or both of the two electronic bands. Using a particular sample at room temperature and with a fixed overpressure of xenon, however, we have measured the intensity of the 123-cm^{-1} band (relative to those of the anion and solvent bands near 660 and 710 cm^{-1}) as a function of the wavelength of the exciting radiation, with the results included in Table IV. Hence, for example, it is apparent that changing the excitation wavelength from 514.5 to 488.0 nm results in a 50% enhancement in the relative intensity of the Raman signal at 123 cm^{-1}, presumably reflecting the admission of the exciting radiation to the tail of the UV band centered at 335 nm. If it is assumed that only one (nondegenerate) excited electronic state r contributes appreciably to the scattering tensor and that the natural half-width of this state is negligible compared with the separation in wavenumber between the electronic band maximum, ν_r, and the exciting radiation, ν_0, the variation in scattering intensity at 123 cm^{-1}, I_{123}, with ν_0 should follow eq 10,[37] where I_{123} is measured

$$I_{123} \propto (\nu_r^2 + \nu_0^2)^2/(\nu_r^2 - \nu_0^2)^4 \qquad (10)$$

relative to I_{ref} associated with the anion/solvent bands. The equation ignores, for simplicity's sake, the factor $(\nu_{123}/\nu_{ref})^4$, which varies by less than 5% over the range of excitation wavelengths used. As revealed in Table IV, the relative intensities calculated on the basis of this equation are generally in good agreement with the experimental results. Only for excitation at $\lambda = 676.4$ nm does the calculated intensity differ markedly from the experi-

(37) Clark, R. J. H.; Stewart, B. *Struct. Bonding* **1979**, *36*, 1.

(38) Howard, W. F., Jr.; Andrews, L. *J. Am. Chem. Soc.* **1975**, *97*, 2956.

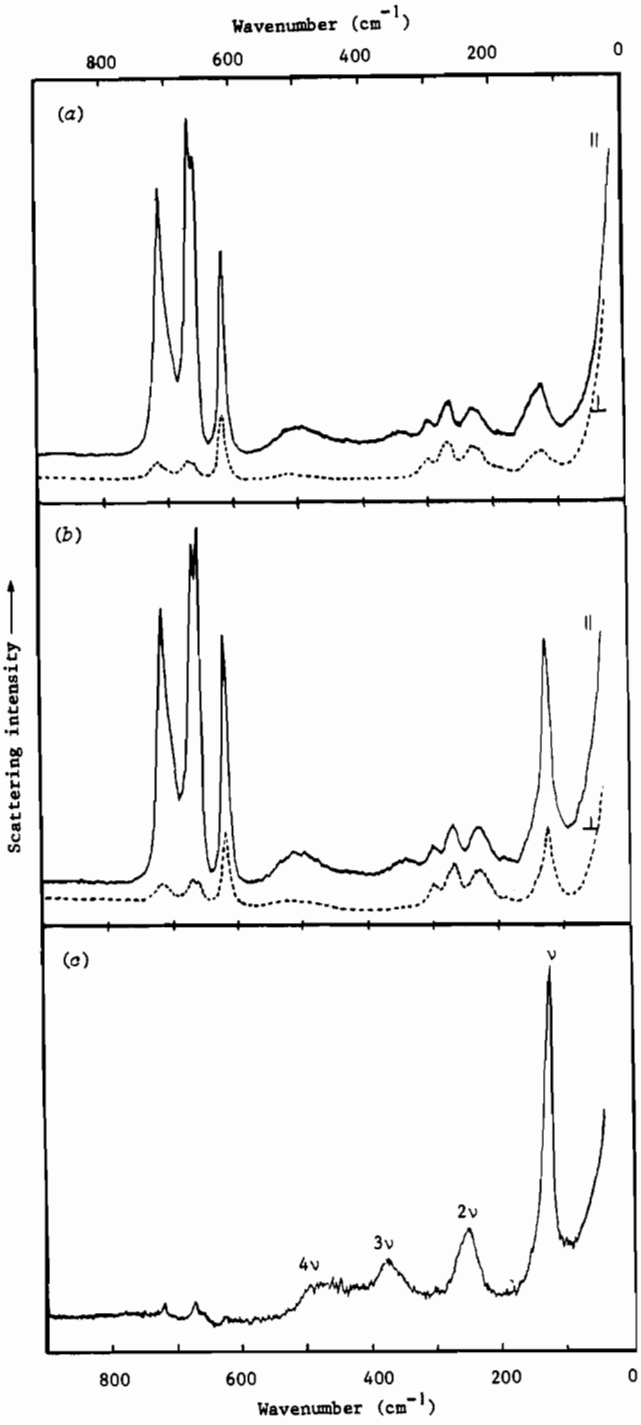

Figure 9. Raman spectra (a) of a solution of $XeF^+Sb_2F_{11}^-$ in antimony pentafluoride solution (pale yellow) excited at $\lambda = 514.5$ nm, (b) of the same solution (green) following the admission of xenon gas to a pressure of 1 atm, also excited at $\lambda = 514.5$ nm, and (c) of the same sample as in (b) but now excited at $\lambda = 676.4$ nm and showing the features characteristic of resonance Raman conditions.

mental figure; in these circumstances it is quite likely that $\nu_r - \nu_0$ is comparable with the natural half-width of the excited electronic state, so that one of the assumptions underlying eq 10 is no longer valid. Indeed, in the region near the maximum of the absorption band, I_{123} is expected to be approximately proportional to the absorption coefficient.[37] On this basis, the ratio of I_{123} at 676.4 to I_{123} at 647.1 nm should be ca. 1.3:1, a prediction quite in keeping with our experimental results. The variations of I_{123} are therefore wholly consistent with the supposition of a common source for the Raman scattering and the electronic bands at 335 and 715 nm.

Table IV. Properties of the Raman Band at 123 cm^{-1} due to the Green Product under Resonance and Preresonance Raman Conditions

exciting radiation		rel intens of 123-cm^{-1} band, I_{123}		measd depolarization ratio, ρ^b
λ (nm)	ν_0 (cm^{-1})	calcd[a]	obsd[b]	
488.0	20 492	1.50	1.5 (0.2)	0.42 (12)
514.5	19 436	1	1	0.37 (7)
568.2	17 599	5.04	3.5 (0.5)	0.36 (6)
632.8	15 803	77.4	30 (5)	0.33 (5)
647.1	15 454	181	45 (5)	0.35 (5)
676.4	14 784	2,068	65 (5)	0.34 (6)

[a] On the basis of eq 10. [b] Estimated error limits of the last digits given in parentheses.

Within the limits of experimental uncertainty, the depolarization ratio of the Raman band at 123 cm^{-1} comes out to be 1:3 and to show no detectable variation with the wavelength of the exciting radiation (see Table IV). Under nonresonant conditions this is the result to be expected for a diatomic oscillator. A simplistic MO approach for Xe_2^+ would assign the 335- and 715-nm absorptions to the transitions $^2\Sigma_g^+ \leftarrow {}^2\Sigma_u^+$ and $^2\Pi_{1/2g} \leftarrow {}^2\Sigma_u^+$, respectively; this would suggest a depolarization ratio of 1:3 for excitation near 335 and a ratio of 1:8 for excitation near 715 nm. When spin–orbit coupling is taken into account,[11b] however, the bands are more appropriately assigned to the transitions $\Pi(^1/_2)_g \leftarrow \Pi(^1/_2)_u$ and $\Gamma(^1/_2)_g \leftarrow \Gamma(^1/_2)_u$ (q.v.); both of these are polarized along the internuclear axis and so should give rise to depolarization ratios of 1:3. Here too, then, the results are totally consistent with the formulation of the scattering species as Xe_2^+.

Conclusions

The partial reduction of the xenon(II) salt $XeF^+Sb_2F_{11}^-$ in the presence of antimony pentafluoride leads to the formation of a green product which is long-lived under a positive pressure of elemental xenon at room temperature; the product is formed reversibly when xenon itself is the reducing agent. Although the product has eluded isolation in the pure state and is not formed in appreciable concentrations in media other than antimony pentafluoride, it has been detected and characterized by its ESR, UV–visible, and Raman spectra. Enrichment in ^{136}Xe and ^{129}Xe establishes that the ESR spectrum is that of the dixenon(1+) cation, Xe_2^+, and correlation of the different spectroscopic properties implies that the same species is also the author of the characteristic UV–visible and Raman spectra. Systematic studies of the intensities of the UV–visible and Raman signals argue that the reversible reaction between xenon and $XeF^+Sb_2F_{11}^-$ conforms to the stoichiometry summarized in eq 9, the redox reaction between 3 mol of xenon and 1 mol of the XeF^+ salt being supplemented by complexation to give, ultimately, the mixed salt $Xe_2^+Sb_2F_{11}^-\cdot XeF^+Sb_2F_{11}^-$. The reaction medium of antimony pentafluoride therefore functions as the source of the $Sb_2F_{11}^-$ anion associated with the Xe_2^+ cation and supports the complex product, most probably as an ion-quartet. Although the lines of the ESR spectrum displayed by Xe_2^+ are rather broad and so could conceal, or in part be affected by, superhyperfine coupling, there is no suggestion of strong coupling to ^{19}F, ^{121}Sb, or ^{123}Sb, and so the interaction with its environment appears to be mainly of a coulombic nature.

The properties we have deduced from the spectra of the Xe_2^+ ion in these conditions are summarized in Table V, together with the corresponding and additional properties of the gaseous ion (as measured experimentally or estimated by quantum mechanical calculations). For comparison the table also includes such data as are available for the isoelectronic diiodine(1–) anion, I_2^-. Not only is the kinship between Xe_2^+ and I_2^- amply demonstrated in this way, but incorporation in the complex $Xe_2^+Sb_2F_{11}^-\cdot XeF^+Sb_2F_{11}^-$ in antimony pentafluoride does not seem to produce undue perturbation of the Xe_2^+ cation. The Σ-like

Table V. Physical Properties Measured and/or Calculated for the Isoelectronic Ions Xe_2^+ and I_2^-

property	Xe_2^+ in SbF_5 in presence of $XeF^+Sb_2F_{11}^-$ [a]	Xe_2^+ gaseous ion expt	Xe_2^+ gaseous ion calcd	I_2^- expt
color	green		green	green
wavelengths of electronic abs bands, λ_{max} (nm)				
$I(^3/_2)_g \leftarrow I(^1/_2)_u$	not obsd		1200[b]	1150[c]
$I(^1/_2)_g \leftarrow I(^1/_2)_u$	715		740[b]	800[c]/740[d]
$II(^1/_2)_g \leftarrow I(^1/_2)_u$	335		348[b]/340[e]	400[c]/385[d]
diss energy, D_e (kJ mol^{-1})		99[f]	96–106[b,g]/66–77[b,h]	84[i,j]/103[i,k]
vibrational freq, ω_e (cm^{-1})	124[l]		122–124[b,g]/110–112[b,h]	114.2–115.6[l]
anharmonic coeff, $\omega_e x_e$ (cm^{-1})	ca. 0.5[l]		0.39–0.47[b,g]/0.44–0.51[b,h]	0.47–0.50[l]
interatomic dist, r_e (pm)	310[m]		303–323[b,g]/323–327[b,h]	316[m]

[a] This work. [b] See ref 11d. [c] See ref 35d; I_2^- formed by X-irradiation of solid doped KI. [d] See ref 35d; I_2^- formed by laser flash photolysis of alcohol solutions containing I_2–I^- mixtures. [e] See ref 11c. [f] See ref 10b. [g] Without spin–orbit coupling. [h] With spin–orbit coupling. [i] See ref 38; $M^+I_2^-$ ion pairs trapped in an Ar matrix (M = alkali metal). [j] Deduced from resonance Raman measurements. [k] Deduced thermochemically. [l] Calculated by the method referred to in ref 38. [m] Calculated from ω_e by the methods given in ref 40.

character of the electronic ground state of Xe_2^+ is endorsed by its ESR properties. Moreover, the weakness of the 1-electron bond is conspicuous (a) in the dissociation energy of 99 kJ mol^{-1} derived from photoionization measurements on the gaseous cation[10b] and (b) in the estimated harmonic frequency of 124 cm^{-1} (cf. I_2^-, 114–116 cm^{-1},[38] and I_2, 215 cm^{-1} [39]). The vibrational frequency signifies a force constant of 59.5 N m^{-1}, and according to the empirical relationships linking force constant and bond length variously proposed by Herschbach and Laurie and Badger,[40] the Xe–Xe bond length would appear to be in the order of 310 pm. This is consistent with the values ranging from 303 to 327 pm calculated on the basis of various theoretical models.[11] It is also in line with the estimate of 331 pm made for the isoelectronic radical XeI in its excited B $^2\Sigma_+$ state (ω_e = 112 cm^{-1}) but much shorter than the interatomic distance of 436 pm characterizing the van der Waals molecule Xe_2 (ω_e = 21.12 cm^{-1}).[41] Even if a crystalline sample of an Xe_2^+ derivative proves to be inaccessible, the interatomic distance in the Xe_2^+ cation may be open to direct determination via EXAFS measurements made on frozen samples similar to those used for most of our ESR and certain of our Raman experiments. The prominent absorption bands centered near 335 and 715 nm find a ready explanation in the dipole-allowed electronic transitions $II(^1/_2)_g \leftarrow I(^1/_2)_u$ and $I(^1/_2)_g \leftarrow I(^1/_2)_u$, respectively, and this assignment receives support from the properties of the Raman scattering excited under resonance or preresonance conditions. Studies of samples at high xenon overpressures may yet reveal the $I(^3/_2)_g \leftarrow I(^1/_2)_u$ transition which is expected to occur in the near-IR region.[11b,35c] Although the ESR and optical spectra appear to follow the same pattern, the system would surely repay MCD measurements over a range of temperatures;[42] hence, one might expect to gain incontrovertible proof that the UV–visible absorber has a paramagnetic ground state.

As to the nature of the complex $Xe_2^+Sb_2F_{11}^-\cdot XeF^+Sb_2F_{11}^-$, we can only speculate. However, the circumstances of our experiments seem to suggest that such complexation is crucial to the long-term survival of Xe_2^+ in appreciable concentrations at room temperature. Just as there appears on the evidence of the ESR spectra to be no strong specific interaction between Xe_2^+ and its neighbors, so it is with the XeF^+ cation, which, if it is perturbed by the complexation, does not betray the effect in either its UV or its Raman spectrum. The conjunction of the two cations Xe_2^+ and XeF^+ may well be significant in producing an aggregate $Xe_2^+\cdots XeF^+$ for which the favorable polarization energy (involving the intervening $Sb_2F_{11}^-$ anions and SbF_5 molecules) actually exceeds the coulombic repulsion. Just such arguments have been shown, for instance, to provide a basis for the stabilization of $F^-\cdots F^-$ and $Cl^-\cdots Cl^-$ ion pairs in aqueous environments.[43]

Experimental Section

(i) Chemical Apparatus and Procedures. To achieve reproducibility, samples were contained in Pyrex glass or quartz apparatus which had been preconditioned by heating under pumping and then exposure for 6–12 h to fluorine gas, typically at a pressure of 200–400 Torr. The apparatus was then evacuated, normally to a pressure $\leq 10^{-4}$ Torr. The construction of the apparatus made limited use of greaseless valves (e.g. those made by J. Young with glass barrels and PTFE keys). To ensure equilibration of the reaction mixture Xe–$XeF^+Sb_2F_{11}^-$–SbF_5, the apparatus was designed with a mixing chamber containing a glass-jacketed magnetic stirrer bar to provide vigorous agitation of the viscous liquid. Some experiments were carried out with apparatus constructed in Teflon–FEP tubing with PTFE couplings and needle valves (Production Techniques Ltd.); this was also conditioned before use by exposure to fluorine gas but at a pressure up to 1 atm. Studies of the Raman spectra of samples made in such apparatus gave results identical in all essential respects to those achieved under rather less rigorous conditions with containment in glass or quartz apparatus. Gas pressures were measured with the aid of a calibrated Bourdon gauge (Budenberg Helicoid), and concentrations were determined by direct weighing and/or volume measurements (made on the neat antimony pentafluoride or samples of the $XeF^+Sb_2F_{11}^-$ solutions).

(ii) Chemicals. The salt $O_2^+Sb_2F_{11}^-$ and other dioxygenyl salts were made from dioxygen, fluorine, and the appropriate Lewis acid by the procedure described previously.[22a,44] Xenon difluoride was prepared by exposure to sunlight of a Pyrex bulb containing Xe and F_2 in the proportions 1.1:1.[45] Samples of the xenon(II) salt $XeF^+Sb_2F_{11}^-$ were produced either from xenon difluoride and antimony pentafluoride[24] or directly by UV photolysis of a mixture of xenon, fluorine, and antimony pentafluoride.[46] The authenticity and purity of these materials were checked by elemental analysis and/or reference to their Raman spectra.[23,24] Antimony pentafluoride was supplied by Alfa Chemicals (stated purity 98%) and purified by distillation in all-glass apparatus. Elemental fluorine was supplied by Air Products and freed from HF by passage over NaF. Elemental oxygen and xenon were normally used as supplied by BOC or Air Products ("Research" grade); samples of ^{136}Xe and xenon enriched in ^{129}Xe (with the composition given in Table II) were similarly used as supplied by Monsanto Research Corp./Mound. The following compounds, from the sources given in parentheses, were purified before use by distillation or sublimation in Teflon-FEP or preconditioned all-glass apparatus: HF (BDH, 99.8%), AsF_5 (prepared from the elements in a Monel bomb[47]), BrF_5 (PCR Inc.), IF_5 (PCR Inc.), HSO_3F (BDH), SbF_3 (BDH), and SO_2 (BDH).

(39) Nakamoto, K. *Infrared and Raman Spectra of Inorganic and Coordination Compounds*, 4th ed.; Wiley-Interscience: New York, 1986.
(40) Herschbach, D. R.; Laurie, V. W. *J. Chem. Phys.* **1961**, *35*, 458. Badger, R. M. *J. Chem. Phys.* **1935**, *3*, 710.
(41) Huber, K. P.; Herzberg, G. *Molecular Spectra and Molecular Structure. IV. Constants of Diatomic Molecules*; van Nostrand Reinhold: New York, 1979.
(42) Piepho, S. B.; Schatz, P. N. *Group Theory in Spectroscopy with Applications to Magnetic Circular Dichroism*; Wiley: New York, 1983.
(43) Jarque, C.; Buckingham, A. D. *Chem. Phys. Lett.* **1989**, *164*, 485. Gao, J.; Boudon, S.; Wipff, G. *J. Am. Chem. Soc.* **1991**, *113*, 9610.
(44) McKee, D. E.; Bartlett, N. *Inorg. Chem.* **1973**, *12*, 2738.
(45) Williamson, S. M. *Inorg. Synth.* **1968**, *11*, 147. The slight excess of Xe was taken to reduce the risk of contamination by XeF_4.
(46) Stein, L. *J. Fluorine Chem.* **1982**, *20*, 65.
(47) Seel, F.; Detmer, O. *Z. Anorg. Allg. Chem.* **1959**, *301*, 113.

(iii) Spectrometers. ESR Measurements were made on samples contained in sealed quartz cells at temperatures ranging from 4 to 300 K. X-Band spectra were recorded with various E-series Varian instruments, viz. a Model E-109 with an E-102 microwave bridge (at Oxford) and a Model E-9 with an E-101 microwave bridge (at Argonne); modulation amplitudes did not exceed 0.1 of the line width, and microwave powers were typically 2 mW or less at 77 K. Temperature regulation was achieved at Argonne with an Air Products Heli-Tran system used in conjunction with an Oxford Instruments temperature controller. Q-Band measurements on samples at ca. 99 K were made with either a purpose-built or a Bruker ER 200D spectrometer in the Department of Chemistry at the University of Leicester.

The UV–visible spectra of antimony pentafluoride solutions of $XeF^+Sb_2F_{11}^-$ at different overpressures of xenon were measured on a Cary Model 14 or a Perkin-Elmer-Hitachi Model 330 spectrophotometer, the sample being contained in a quartz cell with a path length of 1 mm. Searches of the near-IR region were made with a deeply colored sample contained in a cell having a path length of 1 cm and using a Cary Model 14 instrument.

Raman spectra, measured with a Spex Ramalog 5 spectrophotometer, were excited at different wavelengths using the output from a Spectra-Physics Model 165 Ar^+, 164 Kr^+, or 125 He/Ne laser. They were calibrated by reference to the atomic emission lines of a neon lamp housed near the entrance slit to the monochromator. Some of the first samples destined for resonance Raman studies were made in sealed Pyrex glass cells with a length of ca. 5 and a diameter of ca. 2.5 cm; these were rotated at speeds up to 2000 rpm so as to dissipate any heating of the sample while its Raman scattering was being recorded. However, such heating effects appeared to be unimportant, and later measurements were carried out on stationary samples. Intensities of specific Raman bands were estimated by tracing and weighing of appropriate portions of the spectra to assess the areas under the relevant bands.

(iv) Calculations. First-order ESR spectra were simulated using a program devised by one of us (J.R.N.). Simulation at the second-order level was accomplished with the aid of the program SIM,[32] which, with some adaptation,[33] formed the basis of calculations carried out on the Digital VAX Cluster Mainframe computer operated by the Oxford Computing Laboratory. Optimum power regression analysis was performed on an Apple Macintosh microcomputer using standard routines.

Acknowledgments. The work was performed, in part, under the auspices of (i) the Division of Physical Research of the U.S. Energy Research and Development Administration and (ii) the Office of Basic Energy Sciences, Division of Chemical Sciences, U.S. Department of Energy. Another debt is owed to the SERC and its forerunner the SRC both for grants for the purchase of equipment and for the award of studentships (to M.J.C. and A.R.M.). Special thanks are due to Mr. Wayne W. Henderson for his contribution as an undergraduate research participant during the spring term 1979 (see ref 16). We thank also (i) Professor R. J. H. Clark and Drs. D. G. Cobbold and K. Miyano for practical help with the early resonance Raman measurements which were made at University College London and (ii) Professor M. C. R. Symons and Dr. D. Keeble at the University of Leicester for their expert assistance and advice in connection with some of the ESR experiments. To Drs. E. H. Appelman, J. G. Malm, and A. F. Wagner and Professor R. N. Perutz goes the credit for some stimulating discussions of the findings reported here.